https://doi.org/10.1038/s44306-025-00091-2

Interlayer Dzyaloshinskii-Moriya interaction in spintronics

Xupeng Zhao[1] & Jianhua Zhao[2,3] ✉

The indirect interlayer exchange coupling (IEC) between two magnetic layers holds significant importance in development of spintronics. Recently, the interlayer Dzyaloshinskii-Moriya interaction (DMI), antisymmetric counterpart of IEC, has been theoretically predicted and experimentally observed in plenty of magnetic trilayer structures with a nonmagnetic spacing layer. The interlayer DMI favors the orthogonal alignment of the spins or magnetizations throughout the entire multilayer mainly due to the mediation of heavy-metal atoms with strong spin-orbit coupling. Beyond the conventional two-dimensional spin texture driven by intralayer DMI, the existence of interlayer DMI enables the formation of three-dimensional (3D) chiral spin textures. In this article, we aim to provide a comprehensive review of theory model, fundamental properties, manipulation and potential application of interlayer DMI in future spin-based memory and logic devices. Due to the inversion symmetry breaking of the magnetic reversal process, an intriguing phenomenon called chiral exchange bias has been demonstrated. The strength of interlayer DMI exhibits a strong dependence on the azimuthal angle, spacer thickness, spacer material and even magnetization configuration. More importantly, it has been revealed that the interlayer DMI could break the in-plane symmetry and thus facilitate field-free spin-orbit torque switching of perpendicular magnetization. Therefore, this novel interaction provides a fundamental approach for designing and all-electrically manipulation of 3D chiral spin structure. The conclusions and outlooks are also given to inspire more in-depth research and advance the practical applications.

Interlayer exchange coupling (IEC) is an indirect exchange interaction effect between two magnetic layers mediated by conducting electrons in a nonmagnetic (NM) spacer. Over the past four decades, most of the studies on IEC have focused on its symmetric counterpart, i.e., the collinear alignment of magnetization, typically known as Ruderman-Kittel-Kasuya-Yosida (RKKY) interaction, which has laid the foundation of the giant magnetoresistance (GMR) effect and further leads to the emergence of spintronics[1–9]. Notably, the unique properties of RKKY interaction mediated antiferromagnetism (AFM) have been utilized to design synthetic antiferromagnets (SAFs) over the recent years, which open up an intriguing field named SAF spintronics[10–14].

Recently, the antisymmetric counterpart of IEC, interlayer Dzyaloshinskii-Moriya interaction (DMI), has been found to exist throughout the entire magnetic multilayer stack mediated by the NM spacer[15,16]. Generally, DMI is a kind of antisymmetric exchange coupling that arises as a consequence of the spin-orbit coupling (SOC) in the magnetic system lacking inversion symmetry[17–22]. Different from the conventional Heisenberg symmetric exchange interaction that stabilizes the collinear spin or magnetization alignment[23], the magnetic system with DMI favors an orthogonal alignment of adjacent spins in materials. The effective Hamiltonian of DMI can be expressed as $-\boldsymbol{D}\cdot \boldsymbol{S_1}\times\boldsymbol{S_2}$, where $\boldsymbol{D}$ is corresponding to DMI vector, $\boldsymbol{S_1}$ and $\boldsymbol{S_2}$ are two neighboring spins. The DMI in conventional heavy-metal (HM)/ferromagnet (FM) bilayers, namely intralayer DMI or interfacial DMI, is crucial for the formation and stabilization of two-dimensional (2D) chiral spin textures within a magnetic film, such as spin spirals[24], Néel-type domain walls (DWs)[25–27] and skyrmions[28–35].

In 2019, the existence of DMI type of IEC was theoretically predicted in $FM_1/NM/FM_2$ trilayers[36]. Soon after, two publications successfully reported the experimental evidence of this long-range antisymmetric interlayer exchange interaction in SAF multilayers[15,16]. Subsequently, the robust existence of this interlayer antisymmetric effect has been verified in diverse

[1]International School of Microelectronics, Dongguan University of Technology, Dongguan, China. [2]National Key Laboratory of Spintronics, Hangzhou International Innovation Institute, Beihang University, Hangzhou, China. [3]State Key Laboratory of Semiconductor Physics and Chip Technologies, Institute of Semiconductors, Chinese Academy of Sciences, Beijing, China. ✉e-mail: jhzhao@semi.ac.cn

material systems. Overall, interlayer DMI exhibits many unique characteristics. One of the prominent features of interlayer DMI is that it enables three-dimensional (3D) chiral spin structures perpendicular to the film plane[15,16,36], in contrast to the antisymmetric component of the intralayer exchange interactions that leads to 2D spin structures confined within individual magnetic layers[17–22]. Consequently, it is anticipated that the further studies on interlayer DMI will pave the way for the development of 3D spintronic devices with more novel functionalities[37,38].

In this article, we have presented a broad overview of recent progress on interlayer DMI in magnetic multilayers. To elucidate its physical origin, we firstly focused on theoretical model of this long-range antisymmetric interaction. Then, we also presented the basic properties of interlayer DMI, including the chiral exchange bias, and related influence factors, such as azimuthal angle, magnetic configuration, the type of spacer materials and its thickness. In addition, the manipulation mechanisms of interlayer DMI have been mentioned, including azimuthal symmetry engineering and the application of electrical current. Moreover, the currently experimentally verified and theoretically predicted applications of interlayer DMI, mainly consisting of indirect manipulation of 2D spin structure, field-free spin-orbit torque (SOT) switching and enhancing magnon-magnon coupling, have been covered. Finally, the conclusions and outlook towards the practical application of interlayer DMI in spin-based logic and memory devices have been put forward.

Theoretical model of IDMI

For the widely studied intralayer DMI, it describes the coupling of spins S_i and S_j in a FM layer that mediated by a NM HM atom in a neighboring layer[18–22] (Fig. 1a). In 2019, Vedmedenko et al. firstly theoretically predicted the universal existence of interlayer coupling of the Dzyaloshinskii-Moriya type across a spacer based on the three-site Lévy-Fert model[36]. Similar to the physical theory of intralayer DMI, the interlayer DMI in $FM_1/HM/FM_2$ trilayers originates from an antisymmetric counterpart of IEC owing to spin-orbit scattering of conduction electrons in HM layer (Fig. 1b). Similar to intralayer DMI, interlayer DMI can also be described by the three-site Lévy-Fert model[36,39]:

$$D_{ijl}(\vec{R}_{li}, \vec{R}_{lj}, \vec{R}_{ij}) = -V_1 \frac{\sin[k_F(|\vec{R}_{li}|+|\vec{R}_{lj}|+|\vec{R}_{ij}|)+(\pi/10)Z_d](\vec{R}_{li}\cdot\vec{R}_{ij})(\vec{R}_{li}\times\vec{R}_{ij})}{|\vec{R}_{li}|^3|\vec{R}_{lj}|^3|\vec{R}_{ij}|} \quad (1)$$

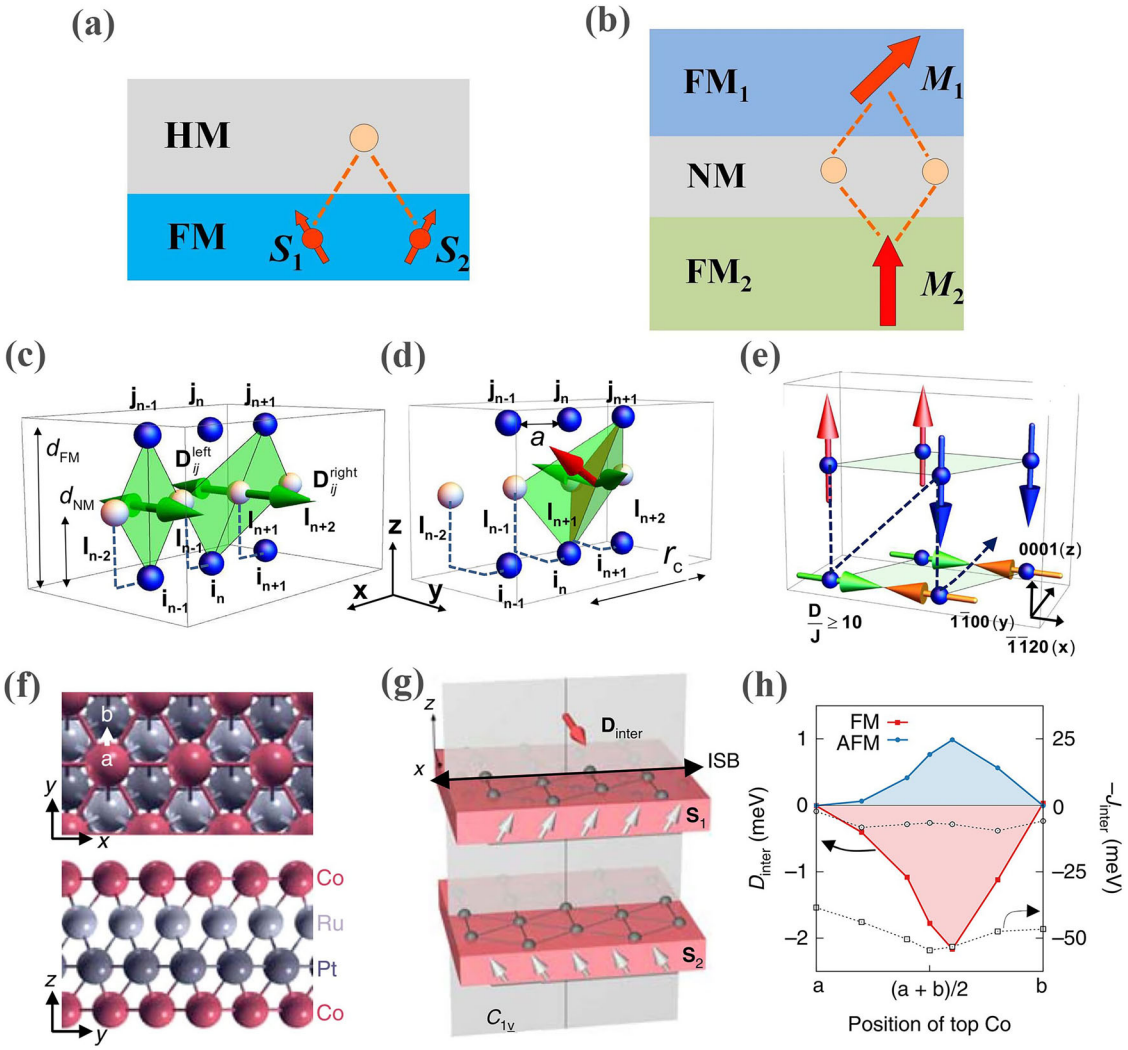

Fig. 1 | The schematic illustration and theoretical model of interlayer DMI. a The physical scenario of intralayer DMI due to HM atom-mediated exchange interactions within a FM layer. **b** The interlayer DMI induced by the antisymmetric IEC between two magnetic layers mediated by conducting electrons in thin NM spacer. **c** The compensation of zero D_{ij}^{eff} in the case of that the magnetic (blue spheres) and NM (gray spheres) atoms lie in the same plane. **d** The formation of non-zero D_{ij}^{eff} when the NM atoms are shifted along the y axis in a hcp stacking. **e** The magnetization configuration in a unit cell with dominating interlayer DMI. Figures **c**, **d** and **e** are reprinted from ref. 36 with permission. **f** Top (top panel) and side(-bottom panel) views of the thin Co/Ru/Pt/Co film. The colored arrows indicate the direction of the considered displacements of the top Co layer. **g** Schematic diagram of the spin canting of initial collinear magnetization due to the interlayer DMI. **h** The strength of J_{inter} (dotted lines) and D_{inter} (solid lines) as a function of the position of the top Co layer. Figures **f**, **g** and **h** are reprinted from ref. 16 with permission.

Where $\vec{R}_{li}$, $\vec{R}_{lj}$ and $\vec{R}_{ij}$ are the distance vectors between corresponding sites. The parameter V_1 is corresponding to the material specific quantity defining the DMI strength, $\boldsymbol{k}_F$ and E_F are the Fermi wave vector and energy, respectively, λ_d is the SOC parameter, Γ the interaction parameter between the localized spins and the spins of conduction electrons, and Z_d the number of d electrons. According to the atomistic Monte Carlo (MC) calculations, this three-site Lévy-Fert model can be extended to $FM_1/NM/FM_2$ trilayers, where the DMI promotes the formation of nontrivial 3D spin textures with both intralayer and interlayer chiralities. The effective DM vector $\boldsymbol{D}_{ij}^{eff}$ for a given ij atomic pair can be described by a sum over all impurities:

$$D_{ij}^{\mathrm{eff}} = \sum_{l} D_{ijl}^{\mathrm{eff}}(\vec{R}_{li}, \vec{R}_{lj}, \vec{R}_{ij}) \tag{2}$$

In most of the one-dimensional cases, individual D_{ijl} is symmetric with respect to any bond and thus add up to zero (Fig. 1d). However, if the nonmagnetic atoms are displaced from their equilibrium positions (Fig. 1e), the $\boldsymbol{D}_{ijl}$ vectors are not compensated anymore. In this case, $\boldsymbol{D}_{ij}^{eff}$ becomes nonzero. The total DM energy for an $FM_1/NM/FM_2$ trilayer can be expressed as:

$$E_{\mathrm{DMI}} = \sum_{ij} D_{ij}^{\mathrm{eff}} \cdot (S_1 \times S_2) \tag{3}$$

When FM_1 and FM_2 are in a perfect FM state but allowed to have any orientation with respect to one another, all $\boldsymbol{D}_{ij}^{eff}$ for a site i in a hexagon cancel out although individual $\boldsymbol{D}_{ij}^{eff}$ is nonzero. However, if magnetization configurations deviate from the perfect collinear alignment, spin and distance variables become mixed and the total E_{DMI} turns to be nonzero. When interlayer DMI $\boldsymbol{D}_{ij}^{eff}$ is much stronger than intralayer Heisenberg exchange coupling $\boldsymbol{J}_{ij}^{intra}$, an AFM row-wise ordering will be formed in both layers (Fig. 1f), according to the MC simulations. In this case, the spin in one layer is perpendicular to the film plane, while the other is parallel to the plane. In practical systems, $\boldsymbol{D}_{ij}^{eff}$ is actually much weaker than $\boldsymbol{J}_{ij}^{intra}$ and then the AFM stripes broaden and the non-collinear alignment of magnetization occurs. The further MC calculations indicate the strength of the interlayer DM energy is calculated to be around 10^{-2} J_{ij} per atom.

Despite the weakness of interlayer DMI per atomic bond, it cannot compete with strong Heisenberg exchange at the atomic scale but can induce chiral coupling between FM layers. Then, the total interlayer DMI energy will create a sizable energy barrier between macroscopic configurations with different chirality, thus leading to a novel phenomenon, i.e., chiral exchange bias. In addition, this long-range antisymmetric interaction is not trivial and seeks to create a 3D spin structure across the magnetic multilayers in all spatial directions, which is significantly different from the intralayer DMI that enables 2D spin structures. Moreover, the basic properties of this interaction rely heavily on the lattice geometry of $FM_1/NM/FM_2$ stacks, the strength of the SOC parameter V_1, and the lateral structure of the multilayer. There is no doubt that this theoretical work opens up an intriguing research topic in the field of spintronics.

Soon later, the theoretical ab initio calculation of interlayer DMI was performed in Co/Ru/Pt/Co system with a collinear magnetization within each magnetic layer[16]. This is achieved by displacing the top Co layer from its high-symmetry position (a and b), resulting in a C_{1v} symmetry structure (Fig. 1f). The antisymmetric DMI arises from a relativistic contribution to the total energy, resulting in a canting angle α between the magnetic moments S_1 and S_2 of the two Co layers (Fig. 1g). The calculations suggested that the presence of an inversion symmetry breaking (ISB), such as a thickness gradient or lattice mismatch, can lead to the interlayer DMI in magnetic heterostructures. In experiment, they have verified that the interlayer DMI can be obtained in samples fabricated by oblique sputtering technique, which generates tilted columnar microstructures with broken inversion symmetry. Figure 1h further presents the calculated strength of both symmetric IEC ($\boldsymbol{J}_{inter}$) and antisymmetric IEC ($\boldsymbol{D}_{inter}$) as a function of the position of the top magnet for an originally FM or AFM interaction between the FM layers. The calculated magnitude of the antisymmetric DMI is smaller than the symmetric interlayer exchange interaction by one to two orders of magnitude. However, the antisymmetric DMI is more sensitive to changes in the symmetry of the crystal lattice, which promotes a chiral magnetization arrangement between the separated magnetic layers. Very recently, Vedmedenko et al. have further conducted the comparison of the theoretical results of interlayer DMI between two magnetic cobalt layers based on ab initio calculations and Lévy-Fert model[40]. A reasonable agreement was observed between these two methods concerning the dependence of the interactions on the position of the spacer layer and the enhancement of the interlayer DMI for higher atomic SOC strength and for the number of valence electrons.

Chiral exchange bias

As predicted by theoretical work[36], the presence of interlayer DMI could contribute to the emergence of chiral exchange bias phenomenon. Notably, the ISB in practical materials could be caused by the thickness gradient, intermixing at the interfaces, lattice defects and even disorder. The experimental observation of interlayer DMI and chiral exchange bias were firstly obtained in Pt/Co/Pt/Ru/Pt/Co/Pt multilayers[16], in which the top and bottom Co layers are indirectly coupled through a Pt/Ru/Pt spacer. By controlling the thickness of Ru interlayer (0.4 or 2.7 nm), the RKKY type IEC can be set as FM or AFM, leading to parallel or antiparallel magnetization alignments, respectively.

Generally, the magnetization switching process of FM films is typically invariant on the inversion of magnetic field direction[41,42]. However, this field-reversal invariance does not hold if the inversion symmetry is broken. For FM/HM bilayers with intralayer DMI, the dynamics of DW expansion turns to be asymmetric under an in-plane field[43–50]. Similarly, the antisymmetric IEC (interlayer DMI) can also break the field-driven magnetization reversal symmetry. In the absence of the interlayer DMI, the application of an in-plane bias field H_{IN} merely facilitates a reduction in the energy barrier for magnetization reversal, irrespective of the switching polarity (see left panels of Fig. 2a, b). As a comparison, the presence of the antisymmetric IEC will introduce a different response of the chiral magnetization configurations to H_{IN}, which can either assist or hinder the magnetization switching depending on the sign of H_{IN} and the specific magnetization configurations. In this case, the energy barriers for magnetization switching from parallel to antiparallel and from antiparallel to parallel alignments, as well as for the switching between down-to-up (D-U) and up-to-down (U-D) processes, turn to be different (see right panels of Fig. 1a, b). As a result, the switching barrier of the magnetization, denoted as the coercive field (H_c), becomes unequal and thus ultimately gives rise to asymmetric magnetic hysteresis loops, leading to the emergence of chiral exchange bias. As shown in Fig. 2c, d, the out-of-plane hysteresis loops become asymmetric in the SAFs both in the parallel and antiparallel magnetization alignments upon the application of H_{IN} of +100 (red) and −100 (black) mT. In the parallel coupling case (top), the difference of switching fields ($\Delta\mu_0 H_{SW}$) between U-D and D-U is found to be approximately 0.7 mT. In the antiparallel coupling case (bottom), the hysteresis loop is biased to the left (right) at +100 mT (−100 mT) with $\Delta\mu_0 H_{SW}$ = 1.1 and 1.4 mT, respectively. This phenomenon reveals the unidirectional and chiral nature of the interlayer DMI, completely different from that of conventional magnetization reversal with symmetric magnetic hysteresis loops[41,42]. Almost simultaneously, experimental evidence of interlayer DMI in a tilted SAF of Co/Pt/CoFeB trilayers was reported[15]. By varying the thickness of top CoFeB layer, the magnetization configuration of the system can be turned from antiparallel, canted, and perpendicular states. Figure 2e, f show both M_z (polar magneto-optic Kerr effect (MOKE)) and M_x (longitudinal MOKE) components of the magnetization as a function of in-plane field. The magnetic trilayer was initially saturated by unipolar (either positive or negative, ~0.4 T) field. It can be seen that the hysteresis loops of the canted CoFeB layer are shifted by nearly ±1.1 mT for the two opposite Co orientations.

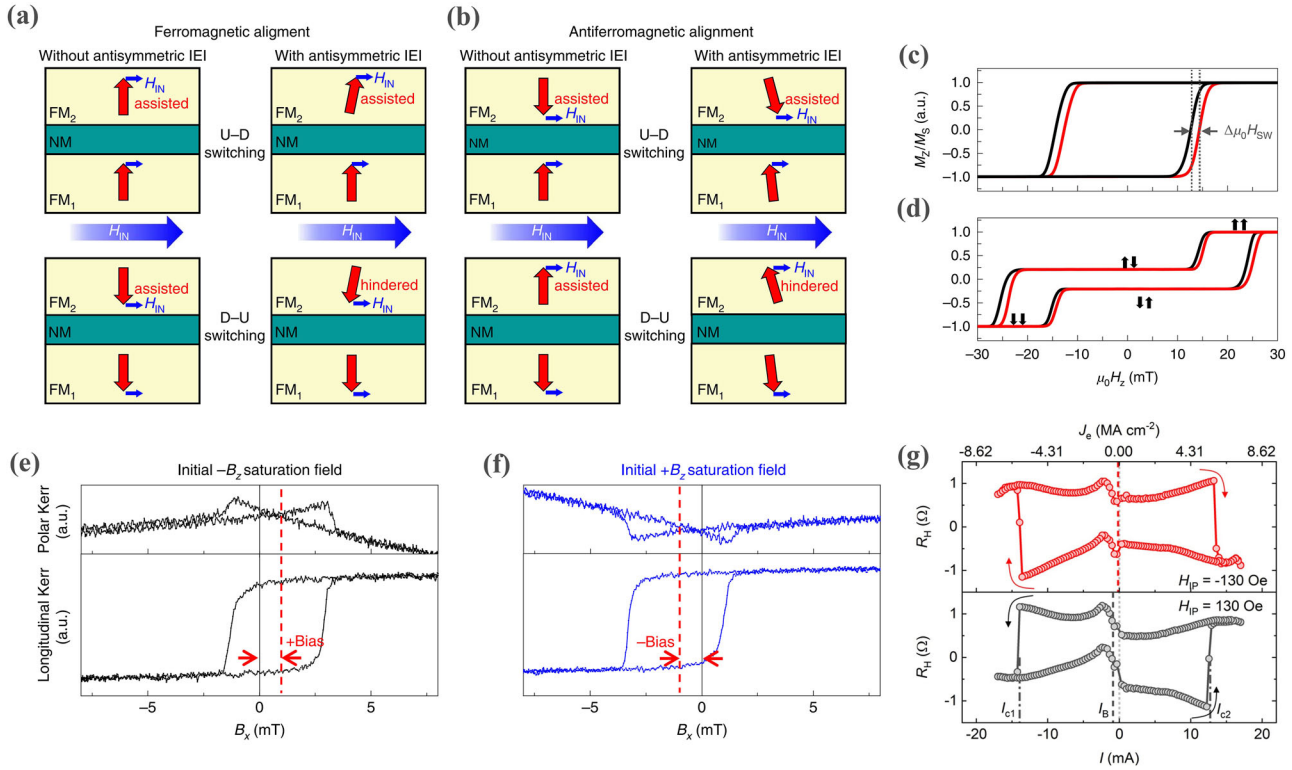

Fig. 2 | The interlayer DMI induced chiral exchange bias. a, **b** Schematics of symmetric and asymmetric switching of perpendicularly magnetized of Pt/Co/Pt/Ru/Pt/Co/Pt with parallel and antiparallel alignments, respectively. **c, d**, Magnetic hysteresis loops for the SAFs with parallel and antiparallel coupling, respectively. The black and red curves indicate the hysteresis loops under the negative and positive in-plane bias field H_{IN} of 100 mT, respectively. Figure **a**–**d** are reprinted from ref. 16 with permission. **e, f** The M_z (polar MOKE) and M_x (longitudinal MOKE) as a function of in-plane field under negative and positive initial saturating field, respectively. Figures **e** and **f** are reprinted from ref. 15 with permission. **g** The asymmetric SOT switching curves under the application of a negative (top panel) and positive (bottom panel) in-plane field. Reprinted from ref. 51 with permission.

Given the symmetry breaking of magnetic reversal induced by interlayer DMI, it is expected that the SOT switching loops may also become asymmetric with respect to switching current density. In 2021, Xiao et al. demonstrated the current-driven asymmetric magnetic switching of SAF CoFeB(1.1 nm)/Ta(1.6 nm)/CoFeB(0.9 nm) structure with interlayer DMI[51]. As shown in Fig. 2g, the deterministic SOT switching of the top CoFeB layer has been achieved under in-plane assisting field H_{IP} of ±130 Oe. Clearly, this current-driven switching is asymmetric with a negative current bias. The asymmetric current-driven SOT switching can be utilized to design SOT devices with selective switching capability that can be turned by H_{IP}. These pioneering experimental efforts have quickly attracts intense interest in the field of spintronics and inspired researchers to conduct more in-depth investigations of interlayer DMI.

In addition to loop shift measurement, other experimental methods have been explored to reveal the chiral magnetic states induced by interlayer DMI, such as neutron scattering techniques and X-ray magnetic circular dichroism photoemission electron microscopy (XMCD-PEEM). In 2022, Wang et al. have systematically characterized the noncollinear magnetic states in perpendicular magnetized SAFs with a structure of Pt/$[Co/Pt]_2$/Co/Pt/NiO/Co/Pt/$[Co/Pt]_2$ by using polarized neutron reflectometry[52]. This research revealed that the maximum angle of the canted magnetic moments for FM coupling can reach as high as 11.5°, which is stronger than that with AFM coupling. In 2023, Fernandez-Pacheco et al. have further observed 360° DW rings with a diameter of 0.5-3.0 μm in Pt/Co/Pt/Ru/Pt/CoFeB/Pt-based multilayer by utilizing the XMCD-PEEM magnetic vector reconstruction[53]. These spin textures are only observed when the interlayer DMI-induced exchange bias field is not perfectly compensated by the magnetic field offset. This work suggested that the interlayer DMI could give rise to complex metastable spin states during magnetic switching.

The azimuthal angle dependence of interlayer DMI

In addition to the observation of chiral exchange bias effect, the azimuthal angle dependence of interlayer DMI has also been investigated systematically in various material systems. In 2019, Kläui et al. presented the azimuthal angle dependence of H_{SW} in Pt/Co/Pt/Ru/Pt/Co/Pt multilayers to reveal the origin of the asymmetric switching behavior[16]. As shown in Fig. 3a, the magnitude of the in-plane field was kept at $|\mu_0 H_{IN}|$ = 100 mT as the azimuthal angle rotates from 0 to 360°. For the Pt/Co/Pt/Ru reference sample with only one FM layer (top panel), the value of H_{SW} is isotropic. However, the magnetic switching exhibits a unidirectional anisotropy for the SAFs with parallel (antiparallel) alignment with symmetric and asymmetric axes aligned along the direction of H_{IN}//75° (150°) and H_{IN}//165° (240°), respectively. This phenomenon suggests the unidirectional nature of the observed interlayer interaction. Notably, the top and bottom magnetic layers own different unidirectional behavior in the case of antiparallel coupling (Fig. 3b). Specifically, the value of $|\mu_0 H_{SW}|$ for the U-D (D-U) is biased to 60° (240°) for the top Co layer, whereas it turns to be biased along the opposite direction for the bottom Co layer. This opposite unidirectional behavior between two magnetic layers directly reveals the chiral nature of the observed unidirectional interlayer DMI effect.

For conventional intralayer DMI, both unidirectional and anisotropic characteristics have been demonstrated[54,55]. Generally, the unidirectional interlayer DMI is most common in plenty-of material systems[16,56,57]. In 2023, Song et al. have firstly observed the existence of anisotropic interlayer DMI with two asymmetric axes in perpendicularly magnetized synthetic FM $[Co/Pd]_9$ multilayers based on both experimental results and theoretical calculations[58]. Figure 3c illustrates the magnetic switching diagram with unidirectional ***D*** (left panel) and anisotropic one (right panel) under in-plane magnetic field H_{IN}. Basically, in the case of unidirectional ***D***, in-plane field H_{IN} will assist or hinder the magnetization switching of a

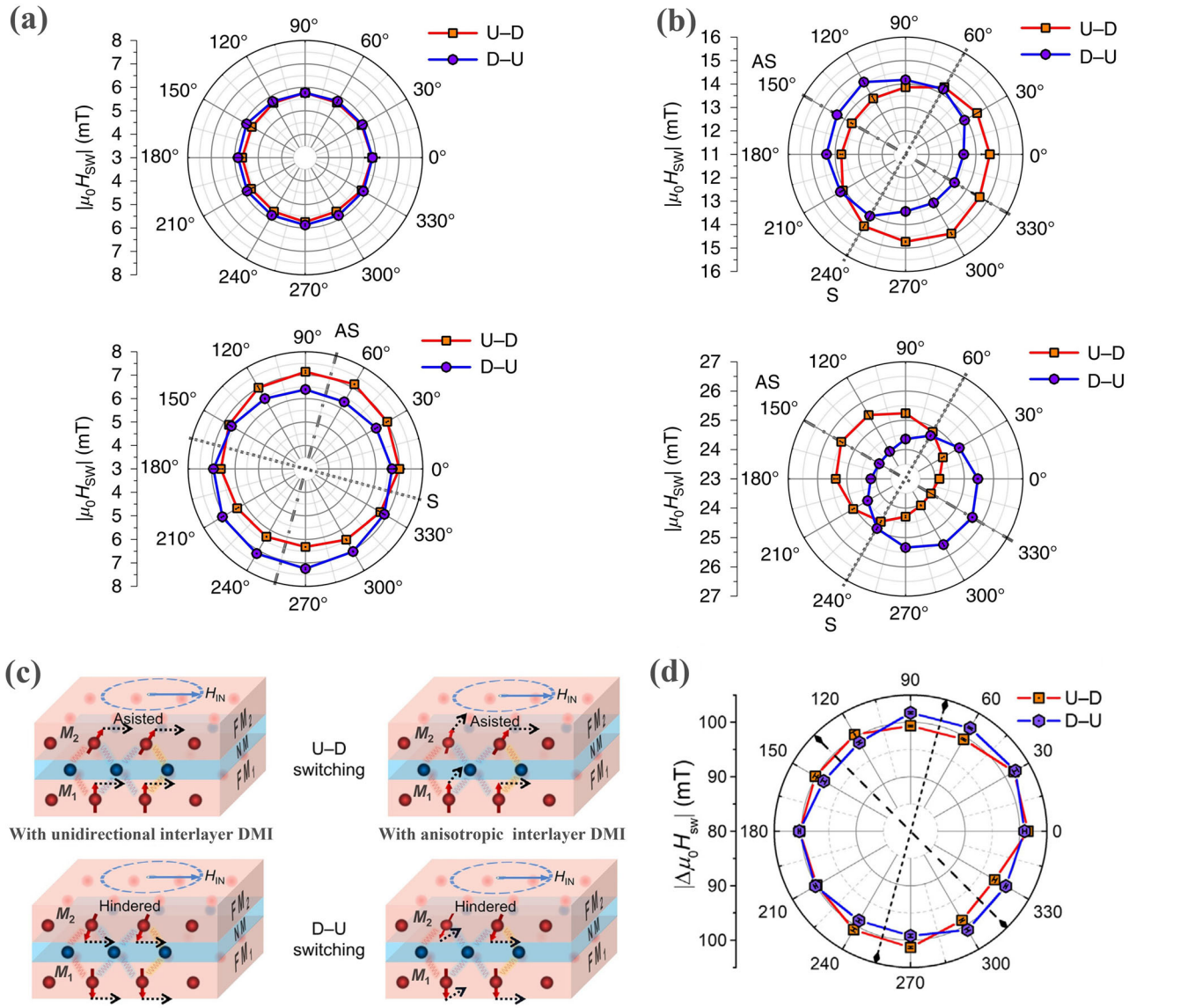

Fig. 3 | The azimuthal angle dependence of Interlayer DMI. a The angle dependence of the switching field of Pt/Co/Pt/Ru (top panel) and FM coupled multilayers of Pt/Co/Pt/Ru/Pt/Co/Pt (bottom panel). **b** Azimuthal angular dependence of the switching field of the top (top panel) and bottom (bottom panel) Co layers of AFM coupled Pt/Co/Pt/Ru/Pt/Co/Pt. Here, AS is referred to the asymmetric axis, i.e., chiral exchange bias field direction. S is corresponding to the symmetric axis, in which chiral exchange bias disappears. The DMI vector (***D***) thus is perpendicular the asymmetric axis AS. Figures **a** and **b** are reprinted from ref. 16 with permission. **c** Schematics diagram of magnetic reversal of synthetic FMs with unidirectional (left panel) and anisotropic (right panel) interlayer DMI vector ***D***. **d** Azimuthal angular dependence of the switching field of $[Co/Pd]_9$ multilayers obtained by MOKE method. Figures **c** and **d** are reprinted from ref. 58 with permission.

perpendicularly magnetized SAFs in one direction, depending on the sign of H_{IN} and the magnetization configurations. While in the case of anisotropic ***D***, the spins of the top and the bottom FMs exhibit multiple directions of non-collinear alignments due to the anisotropic nature of ***D*** and thus there are multiple directions to assist or hinder the magnetization switching. As shown in Fig. 3d, it can be seen that there are two directions of relative shift with respect to the U-D and D-U switching, and the angle between these two asymmetric axes labeled by the dot lines is around 60°. Based on the first-principle calculations, the anisotropic D that leads to asymmetric switching behaviors in $[Co/Pd]_9$ with two orientations is attributed to the two highly symmetric directions of Co layer.

Interlayer DMI with orthogonal magnetic configuration

Most of investigation of interlayer DMI has been conducted in SF or SAF with parallel or antiparallel alignment of perpendicular magnetization. It has been experimentally revealed that the magnitude of interlayer DMI is strongly dependent on the specific magnetization configuration[15]. In 2021, Gambardella et al. focused on the critical role of orthogonal magnetization configuration in maximizing the interlayer DMI strength between Co and TbFe layers with a Pt spacer[59] (Fig. 4a). According to the anomalous Hall curves (Fig. 4b), there is a natural orthogonal magnetization configuration between out-of-plane (OOP) magnetized TbFe and in-plane (IP) magnetized Co. The measurement configuration is presented in Fig. 4c, in which the external magnetic field was swept along in-plane azimuthal angle φ_B with an oblique angle θ_B. The maximum difference of coercive force (ΔB_c) was observed with the field tilted toward $\varphi_B = 135°$ and 315°, the corresponding Hall resistance curves is given in Fig. 4d. According to the φ_B dependence of B_c (Fig. 4e), the magnitude of ΔB_c varies as a sine function of φ_B, which implies a unidirectional behavior. To investigate the influence of interlayer DMI on the IP Co layer, the longitudinal resistance R curve was measured with the in-plane field applied at $\varphi_B = 0°$. The shift ΔB_s between the two curves corresponds to a net bias field acts on $\boldsymbol{M}_{Co}$, and the value of

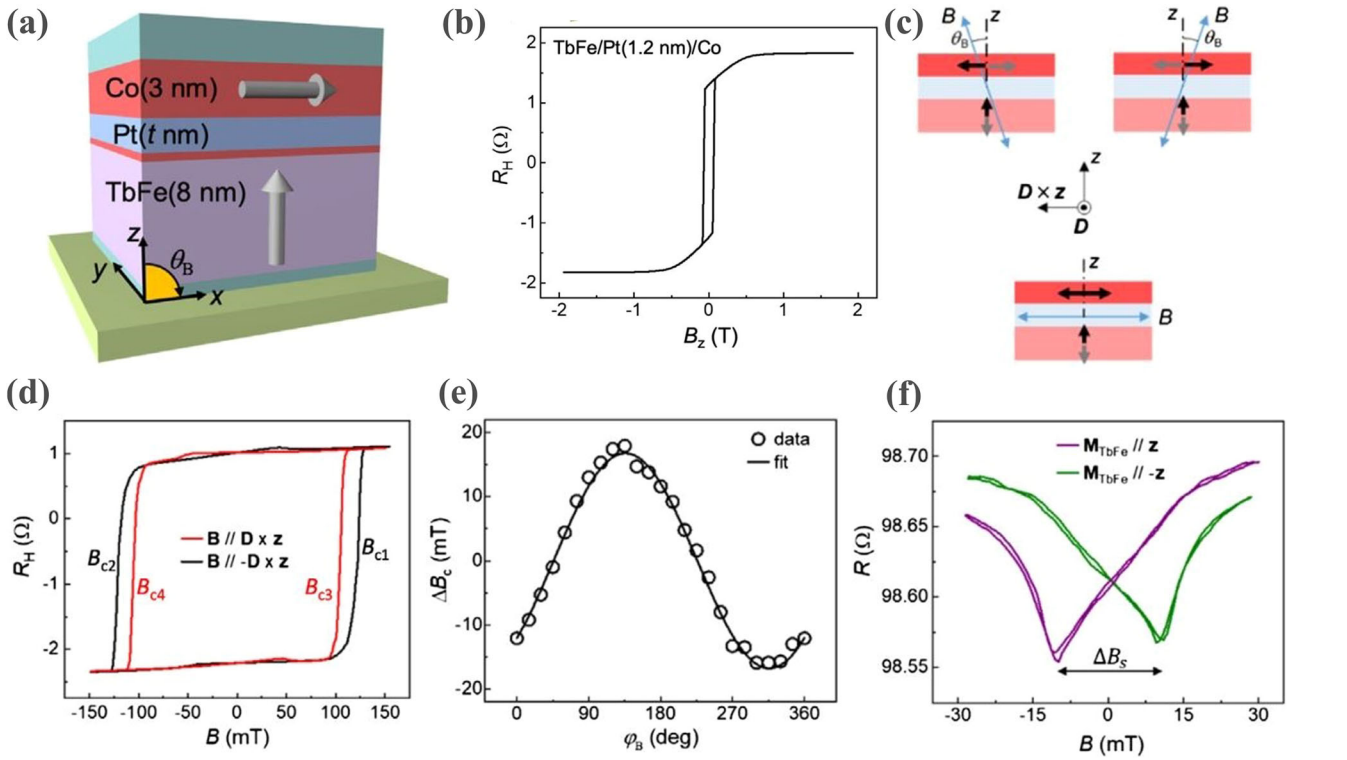

Fig. 4 | The interlayer DMI with orthogonal magnetization. a Illustration of the TbFe/Pt/Co based magnetic multilayer with orthogonal magnetic easy-axis. **b** The out-of-plane Hall resistance loops of TbFe/Pt (1.2 nm)/Co sample. **c** Schematics of the field sweep measurements with tilt angle favoring and opposing the interlayer DMI (top left and right, respectively). The bottom diagram shows the geometry employed for the magnetoresistance measurements. **d** The Hall resistance curves of TbFe/Pt(1.5 nm)/Co measured during a field sweep at $\theta_B = 15°$ tilted along $D\times z$ (red line, initial $\varphi_B = 315°$) and along $-D\times z$ (black line, initial $\varphi_B = 135°$). **e** The coercivity difference ΔB_c as a function of φ_B. **f** Magnetoresistance curves as a function of the in-plane field for two different orientations of M_{TbFe}. Figures **a**-**f** are reprinted from ref. 59 with permission.

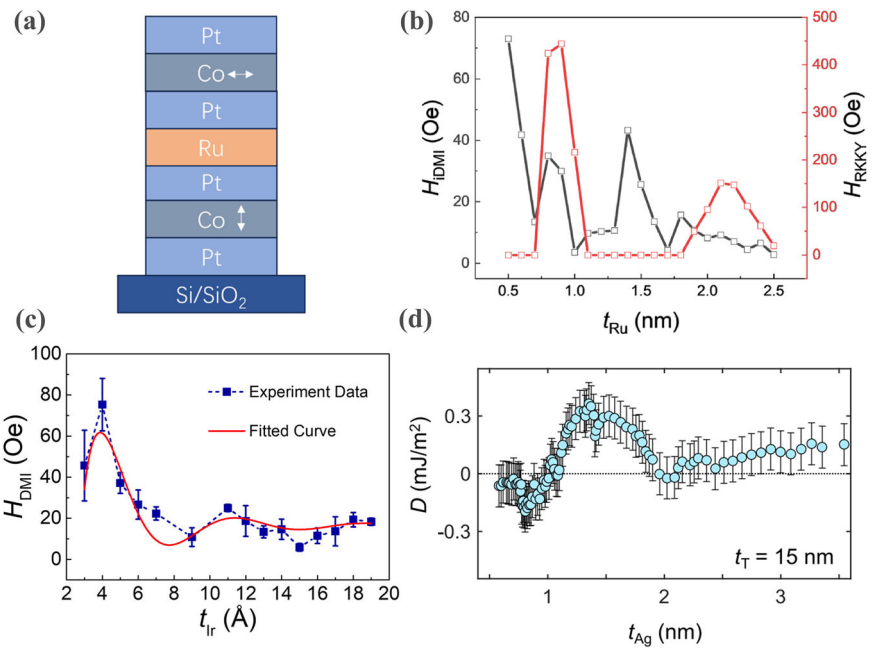

Fig. 5 | The oscillation decay trend of interlayer DMI strength. a The sample stacking structures of Pt(3)/Co(0.5)/Pt(0.5)/Ru(t_{Ru})/Pt(0.5)/Co(2)/Pt(3) (thickness in nm) with T-type magnetic configuration. **b** The strength of H_{iDMI} and H_{RKKY} as functions of the thickness of Ru spacer (t_{Ru}). Figures **a** and **b** are reprinted from ref. 62 with permission. **c** The strength of H_{DMI} as a function of the thickness of Ir spacer (t_{Ir}) in Pt/Co/Pt/Ir/Pt/Co/Pt multilayer. Reprinted from ref. 56 with permission. **d** Ag thickness dependence of the interlayer DMI in Co/Ag/Co trilayer. Reprinted from ref. 65 with permission.

B_{DMI} acting on the Co layer can be estimated by using the formula $B_{DMI} = \Delta B_s/2$. The obtained maximum value of interlayer DMI field B_{DMI} reaches up to 13 mT, corresponding to $E_{DMI} \approx 44$ μJ/m^2, which is significantly larger than those found in previous work[15,16,56,57] and reveals the potential of utilizing orthogonal magnetic configurations to enhance the interlayer DMI in spintronic devices. The enhanced interlayer DMI strength has also been observed in $D0_{22}$-Mn_3Ga/Pt/Co trilayers with orthogonal magnetization[60].

According to theoretical work based on Lévy-Fert model or ab-initio calculations[16,36,40], the corresponding strength of interlayer DMI ***D*** per

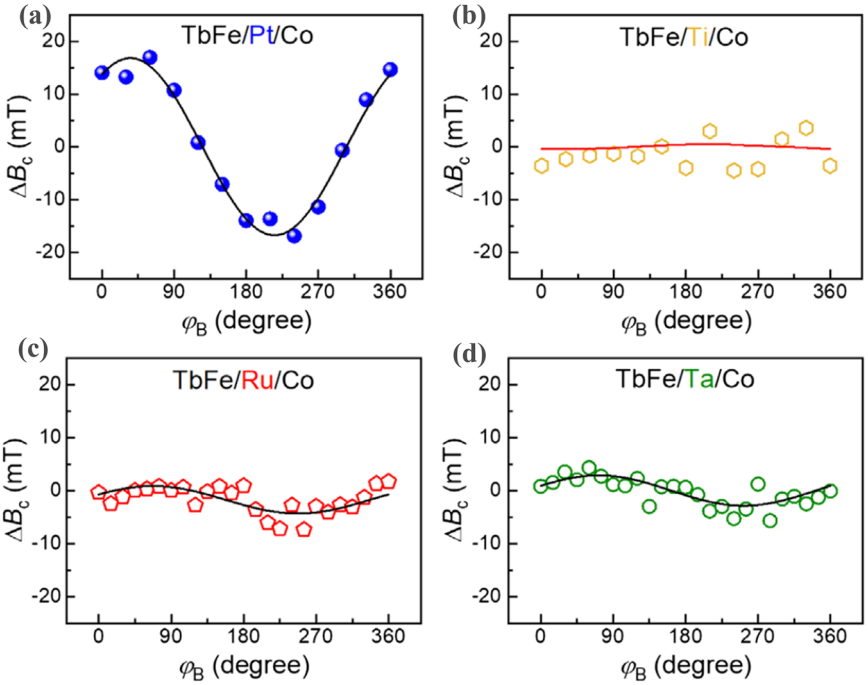

Fig. 6 | The comparison of interlayer DMI strength with different spacer materials. a–d The chiral exchange bias field (ΔB_c) as a function of in-plane azimuthal angle φ_B for TbFe(8 nm)/Co(0.4 nm)/X(1.7 nm) samples with Pt, Ti, Ru, and Ta spacers, respectively. Figure **a–d** are reprinted from ref. 59 with permission.

atomic bond is on the order of meV (~1.602×10^{-22} J). In experimental measurements[57], the magnitude of $\boldsymbol{D}$ can be regarded as the interlayer DMI energy per unit area of the film and thus possesses the unit of J/m^2 or erg/cm^2. In principle, in addition to the film thickness, the conversion between the strength of microscopically calculated $\boldsymbol{D}$ and macroscopically measured one requires the consideration of many microscopic factors, such as the bond density, compensation state and disorders.

Oscillatory behavior of interlayer DMI

In principle, the symmetric RKKY interaction exhibits an oscillatory nature that favors either parallel or antiparallel alignment of the magnetization of the FMs, depending on the critical thickness of NM spacer[1–9]. As both the antisymmetric interlayer DMI and symmetric RKKY can be regarded as a sub-item of the total IEC, their oscillatory behavior may share a similar physical origin. According to the theoretical calculation, the interlayer DMI coupling between two magnetic atoms shows an oscillating decay trend with the distance between them[16,36,40]. The scattering effect of impurities dominates both RKKY and DMI couplings. Consequently, it is expected that the oscillatory behavior of interlayer DMI shares the same period as RKKY. In early studies, the strength interlayer DMI typically exhibits a monotonous decrease trend with spacer thickess[59–61]. Similar to the conventional RKKY interaction, these experimental results indicate that crystalline defects and roughness may potentially exert adverse effects on the observation of oscillatory behavior.

In 2023, Han et al. first presented a comprehensive investigation of the oscillatory behavior of interlayer DMI and its inside correlation with RKKY interaction in magnetic multilayers of Pt/Co/Pt/Ru/Pt/Co/Pt structures[62], as illustrated in Fig. 5a. Both the spacer thickness dependence of interlayer DMI in a T-type structure and RKKY interaction in collinear-type structures are systematically characterized. The magnetization configuration of the bottom and top FM layers is controlled by varying the Co sublayer thickness in top Pt/Co/Pt. The top Pt (0.5)/Co (0.5)/Pt (3 nm) shows good perpendicular magnetic anisotropy (PMA), while it turns into in-plane magnetic anisotropy (IMA) when the thickness of Co is 2 nm. Based on the loop-shift measurement mentioned above, the interlayer DMI strength (H_{iDMI}) can be obtained. Meanwhile, the shift field of the minor loop marks the RKKY interaction induced effective field (H_{RKKY}). Figure 5b clearly shows the deduced value of H_{iDMI} and H_{RKKY} as the function of spacer thickness t_{Ru}. Obviously, oscillation decay tendency has been obtained with the average period of around 0.5 nm. Moreover, it can be seen that the oscillatory behavior of interlayer DMI and RKKY interaction is roughly synchronous. That is, both interlayer DMI and RKKY interaction exhibit an oscillation-damping behavior with the increase of spacer thickness, indicating a gradual weakening of the IEC strength between magnetic layers. Therefore, the experimental results are well consistent with the theoretical expectation. Soon later, other groups have also reported the observation of oscillation decay characteristics of interlayer DMI in other sample stacking structures[56,63–65]. As plotted in Fig. 5c, d, the oscillation decay behavior of interlayer DMI strength was also observed in Pt/Co/Pt/Ir/Pt/Co/Pt and Co/Ag/Co multilayers[56,65]. Worth mentioning, similar to conventional RKKY interaction, both the sign and amplitude of interlayer DMI exhibit periodic oscillatory behavior in Co/Ag/Co multilayers. All of these results have suggested a strong physical relation between interlayer DMI and RKKY interaction[40].

The spacer materials dependence on interlayer DMI

It is well-established that the intensity of RKKY interaction relies on the type of spacer material in FM_1/NM/FM_2 trilayers, in which the NM layer is usually Cu, Cr, or Ru[1–9]. Among these spacer materials, Ru is the most widely adopted to introduce a strong RKKY interaction. Hence, it is significant to explore the spacer material dependence of interlayer DMI. In 2021, Gambardella et al. have shown the experimental comparison results of interlayer DMI strength in TbFe/NM/Co trilayers with varied spacer of HM (Pt, Ta), light-metal Ti, and Ru[59]. Figure 6a-d show the corresponding chiral exchange bias field ΔB_c measured by performing field sweeps at different angles φ_B. Based on the sinusoidal fitting, the maximum interlayer DMI field B_{DMI} reaches to around 13 mT for the sample with Pt spacer, corresponding to $E_{DMI} \approx 44$ μJ/m^2. However, the magnetite of B_{DMI} is only 0.5 mT for Ti, 2.6 mT for Ru, and 2.9 mT for Ta. Obviously, these values are far smaller than that of Pt. The relatively small interlayer DMI observed in Ti and Ru could be attributed to their weak SOC. Despite the large atomic SOC of Ta, it generates much smaller interfacial DMI compared with Pt[66]. The weaker SOC and interfacial DMI of these alternative materials result in a significant reduction of interlayer DMI intensity. Therefore, this work has highlighted the crucial role of the bulk SOC of the spacer in the formation of interlayer DMI.

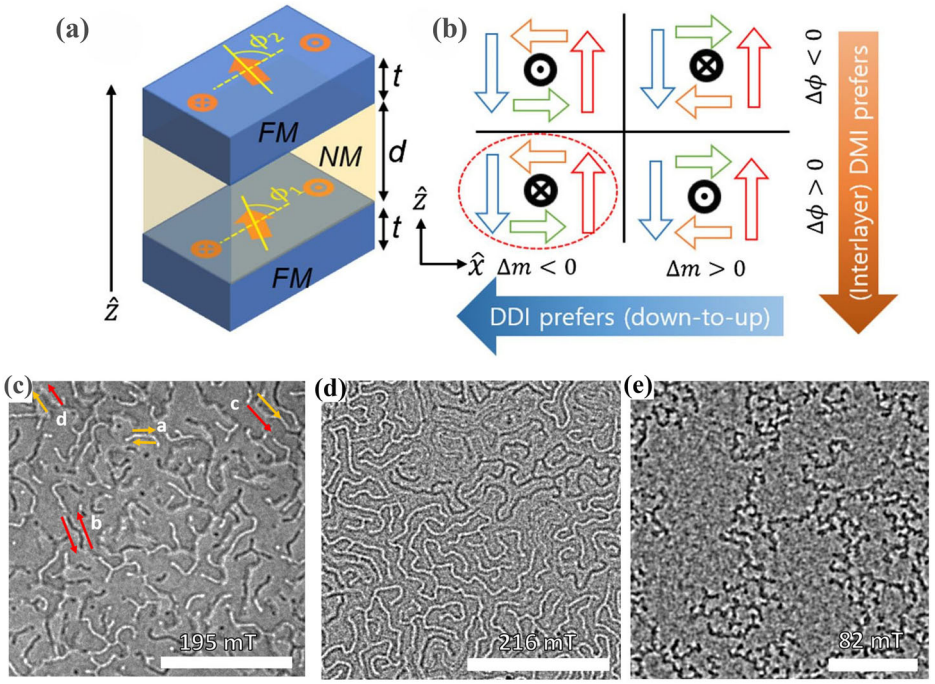

Fig. 7 | Manipulation of Bloch chirality of DWs by utilizing interlayer DMI. a Schematic illustration of a typical multilayer with interlayer DMI. **b** Schematic diagram of a preferential Bloch chirality due to the influence of an assumed negative interlayer DMI and dipole-dipole interactions (DDI). Here, the colored arrows indicate the spin orientation in the DW structure, and ⊗(⊙) presents the average DW magnetization lying along the -y ($+y$) direction. **c**–**e** The domain contrast for the $[Co_7Pd_5]_{15}$, $[Co_7Pd_5]_{30}$ and $[Co_9Pd_{10}]_{30}$ samples obtained by LTEM. Figures **a**-**e** are reprinted from ref. 67 with permission.

Apart from the well-accepted contribution of atomic SOC in HMs mentioned above, Vedmedenko et al. firstly revealed that the strong interfacial Rashba-type SOC will also contribute to a considerable interlayer DMI in 2023[65]. A scissor-like in-plane state between the magnetization vectors of the two Co layers that follows a predefined chirality was obtained in Co/Ag/Co trilayers. Meanwhile, the estimated interlayer DMI strength with in-plane chirality is on the order of ~0.1 mJ/m^2, comparable to the best results with HM Pt spacer. The observed strong interaction was attributed to a combination effect of inversion symmetry breaking and strong Rashba SOC at Co/Ag interfaces or from the Lévy-Fert three-site coupling via Co impurities. The in-plane chirality and strong interlayer DMI strength exhibit potential applications in field-free SOT switching, chiral giant magnetoresistance effect, and other novel spintronic devices. Moreover, this study expands the class of materials exhibiting interlayer DMI to light NM metals with weak atomic SOC, paving the way for further exploration and optimization of interlayer DMI in various spacer material systems. In 2024, they have also investigated the interlayer DMI in Co/NM/Co with four different spacer materials (Cu, Ag, Pt, and Au) based on both Lévy-Fert model and ab initio calculations[40]. An increased DMI strength can be obtained for heavier elements with a stronger atomic SOC, and the highest value can be obtained for an Au spacer. It has also revealed that the contribution of the magnetic Co atoms to the interlayer DMI partially compensates that of the NM spacer.

Application of interlayer DMI in spintronics

Despite the interlayer DMI being a relatively new effect in the field of spintronics, it has been demonstrated to possess intriguing applications beyond the construction of 3D topological spin structures and chiral exchange bias in magnetic multilayers[15,16,36]. Additional applications contain the indirect manipulation of intralayer spin structures, facilitating field-free SOT switching, and introducing strong magnon-magnon coupling[67–69]. Therefore, it is reasonably expected that the interlayer DMI could play multiple roles in the design and manipulation of cutting-edge spintronic devices.

Indirect manipulation of intralayer spin structure

In 2021, Yang et al. reported that interlayer DMI could break the degeneracy between the two Bloch chiralities of DWs in relatively thick multilayers[67]. A simple model considered in this work was based on the magnetic trilayer structure in which two FM layers are separated by a NM spacer (Fig. 7a). As presented in Fig. 7b, a preferential rotation of the magnetization through the multilayer thickness and a certain type of Bloch chirality will be formed due to the combined influence of interlayer DMI and dipole-dipole interactions (DDI). The DDI preferentially favors a flux closure state, selecting the initial magnetization orientation at both surfaces, whereas interlayer DMI preferentially favors one direction of rotation between the surfaces. The symmetry analysis of the interlayer DMI indicates that the normal component (D_z) is crucial for breaking the degeneracy between Bloch chiralities.

The experimental evidence supporting the theoretical predictions was obtained through Lorentz transmission electron microscopy (LTEM) measurements of Co/Pd multilayers. Figure 7c-e show the typical magnetization states after saturation and relaxation to the indicated field values for the $[Co_7Pd_5]_{15}$, $[Co_7Pd_5]_{30}$, and $[Co_9Pd_{10}]_{30}$ samples, respectively. For $[Co_7Pd_5]_{15}$ with a total magnetic thickness of 18.7 nm, no obvious asymmetry from bright and dark domains is present. However, a clear population asymmetry can be observed in $[Co_7Pd_5]_{30}$ with a thickness of 36.7 nm. The probability of clockwise (CW) domains, P(CW) was measured as 0.79 ± 0.10. For $[Co_9Pd_{10}]_{30}$, only CW domains were observed. As a result, a clear population asymmetry of Bloch DWs was achieved with a preference of CW rotations, which becomes more pronounced in thicker films and multilayers with higher magnetic volume, consistent with the theoretical model's dependence on demagnetization energy. In principle, the observed preferred Bloch chirality in Co/Pd multilayers is a result of the interplay between interlayer DMI and demagnetization fields. By tuning the strength of interlayer and intralayer DMI, it is possible to design magnetic systems with desired Bloch chirality, potentially mitigating undesired effects like the skyrmion Hall effect. This work has confirmed the feasibility of indirectly controlling 2D spin structure in magnetic multilayers by utilizing interlayer DMI.

Interlayer DMI-assisted field-free SOT switching

The next significant step towards the utilization of interlayer DMI in spintronic devices is the realization of field-free SOT switching[61,63,68,70,71]. Generally, the SOT effect has been proven to be a valid way to electrically manipulate the local magnetization[72–74], which has been regarded as an alternative writing mechanism in magnetic random access memory

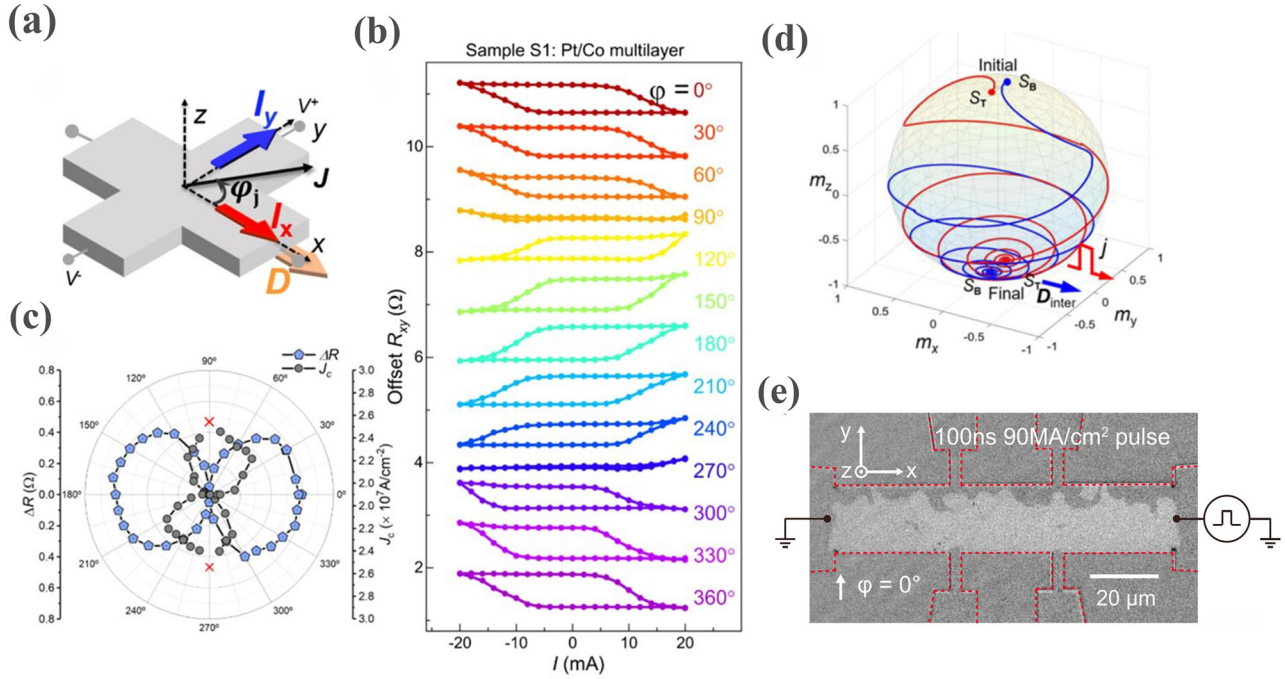

Fig. 8 | Interlayer DMI induced field-free SOT switching. a The measurement configuration of SOT switching in Pt/Co/Pt/Co/Pt and Pt/Co/Pt/Ir/Pt/Co/Pt based Hall devices. **b** Field-free SOT switching loops at different φ_j for the FM coupled Pt/Co/Pt/Co/Pt sample. The switching loops disappeared at $\varphi_j = 90°$ and 270°. **c** Resistance change (ΔR) and critical current (J_c) of the switching as functions of φ_j. **d** Switching dynamics driven by a pulse current parallel to ***D***. Figures **a**-**d** are reprinted from ref. 68 with permission. **e** MOKE image of the Hall device after the application of a current pulse. Reprinted from ref. 71 with permission.

(MRAM)[75,76]. In principle, the spins with in-plane polarization cannot break the in-plane inversion symmetry for a perpendicular magnetization and an external in-plane magnetic field is typically required to assist the deterministic switching[77–80]. However, the introduction of an in-plane assisting field not only complicates the device structure but also increases the write power consumption. So far, several approaches have been proposed to address this issue, including lateral asymmetry[14,81–85], local effective in-plane field[86–90], out-of-plane spin polarization[91], and gradient effect[92–96]. At present, there are still some specific technical drawbacks that hinder their broad application in wafer-scale manufacture.

In 2022, Han et al. first found that interlayer DMI effect could break the in-plane symmetry and facilitate deterministic SOT switching of a perpendicular magnetization[68]. Based on the symmetry analysis, it was found that the existence of interlayer DMI introduces an antisymmetric coupling between adjacent magnetic layers, thus breaking the mirror symmetry of the system. When a current is applied parallel to the ***D***, the system symmetry is reduced, allowing the deterministic SOT switching of the perpendicular magnetization. By varying the angle between the current direction and the ***D***, the magnitude and direction of the SOT switching can be controlled. When the current is applied perpendicular to the ***D***, the symmetry-breaking effect of the interlayer DMI is neutralized. In this case, the deterministic SOT switching disappears. The field-free SOT switching was successfully realized in both FM coupled Pt/Co/Pt/Co/Pt and AFM coupled Pt/Co/Pt/Ir/Pt/Co/Pt structures with the existence of interlayer DMI. Specifically, a symmetry-breaking law of ***j***//***D***, where ***j*** represents the applied current density and ***D*** represents the vector of the interlayer DMI, was theoretically elaborated upon and then experimentally verified. The experimental setup of SOT switching is presented in Fig. 8a, in which I_x and I_y were applied simultaneously to adjust the direction (φ_j) of the current density in the cross region relative to the ***D*** vector. According to the SOT switching loops for various φ_j values (Fig. 8b), field-free SOT switching has been achieved when $\varphi_j \neq 90$ or 270°. The degree of switching (ΔR at $I_0 = 0$ mA) and the critical current (J_c) as functions of φ_j is shown in Fig. 8c. Obviously, ΔR_{xy} (J_c) is maximized (minimized) at ***j***//***D*** and turns to be zero (divergent) at ***j***⊥***D***. In brief, this phenomenon can be interpreted that the interlayer DMI energy can be reduced in the case of ***j***//***D*** by choosing the preferred magnetization alignment and then deterministic SOT switching occurs.

Figure 8d further presents the critical SOT switching dynamics obtained by micromagnetic simulation performed by MuMax3. The simulation has demonstrated that the presence of interlayer DMI leads to deterministic switching of the perpendicular magnetization in both FM and AFM coupled samples with the absence of an external field, in agreement with the experimental results. In comparison to previous field-free switching methods that require additional functional layers or asymmetric designs, the interlayer DMI effect enabled field-free switching is an intrinsic property of Pt/Co systems. In 2023, Zhao et al. also demonstrated the field-free SOT switching in Pt/CoB/Pt/Ru/Pt/CoB/Pt SAF based on the measurement setup that interlayer DMI ***D*** is parallel to the electrical current[71]. The corresponding domain structure after pulse application observed by MOKE microscopy is shown in Fig. 8e. It can be seen that the top CoB layer is switched from the down to the up state in nearly 80% of the Hall bar area under zero external field. All of these results reveal that the interlayer DMI could serve as an effective symmetry-breaking mechanism that facilitates the implement of all-electrically SOT switching.

Interlayer DMI induced ultrastrong magnon-magnon coupling

Magnon-magnon coupling has drawn much interest in the field of spintronics due to its potential for quantum engineering[97–105]. How to realize strong magnon-magnon coupling is a crucial issue for enhancing the efficiency of quantum information processing. In addition to the aforementioned applications, in 2024, Yu et al. have theoretically predicted that interlayer DMI can also break the rotational symmetry of SAF systems and lead to the emergence of ultrastrong magnon-magnon coupling in SAFs[69]. Based on the micromagnetic simulations, it was found that the coupling strength can be effectively tuned by manipulating the orientation of the interlayer DMI vector *D*, as well as the material parameters of the SAF, including the magnetic anisotropy field, effective interlayer DMI field, and effective RKKY interaction field. Notably, a significant enhancement in coupling strength occurs when the total magnetic anisotropy field

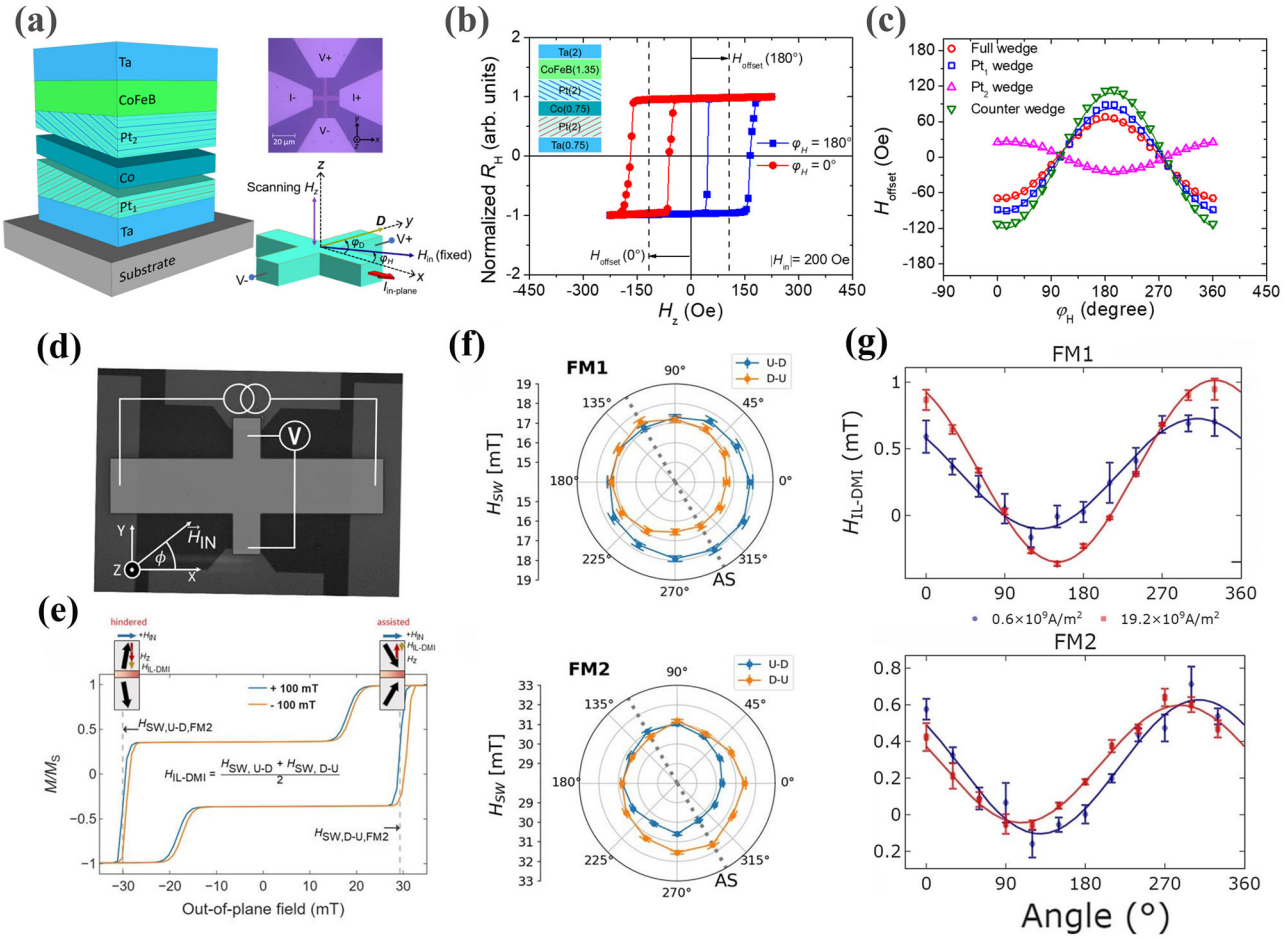

Fig. 9 | The modulation of interlayer DMI. a The illustration of the counter-wedge sample by using OAD technique and the corresponding loop-shift measurement setup. **b** The R_H-H_z loops of the counter-wedge sample measured at $\varphi_H = 0°$ and $\varphi_H = 180°$. **c** The offset field H_{offset} as a function of φ_H for different wedge growth conditions. Figures **a–c** are reprinted from ref. 108 with permission. **d** The measurement setup for characterizing the current dependence of interlayer DMI. **e** Magnetic hysteresis loops under positive and negative in-plane field of 100 mT, respectively. **f** The switching field dependence on ϕ for FM_1 and FM_2, respectively, under a low current density of 0.6×10^9 A/m^2. **g** The azimuthal dependence of $H_{IL\text{-}DMI}$ under a current density at 0.6×10^9 A/m^2 and 19.2×10^9 A/m^2 for both FM_1 and FM_2. Figures **d–g** are reprinted from ref. 109 with permission.

approaches zero. In this case, even a relatively small interlayer DMI can induce an ultrastrong magnon-magnon coupling. The maximum normalized coupling strength g/ω_0 reaches up to 0.5. Very recently, other groups have also theoretically studied the influence of interlayer DMI on the dynamics of spin waves in magnetic multilayers. It is theoretically predicted that interlayer DMI could change the frequencies of the fundamental ferromagnetic resonance spectra (FMR) modes, which is different from conventional intralayer DMI[106]. Additionally, interlayer DMI could also lead to asymmetric spin-wave propagation behavior between the two FM atomic layers[107]. These findings indicate the significant role of interlayer DMI in the advancement of magnon or spin wave-based quantum engineering techniques.

The manipulation of interlayer DMI

The ability to control and tune interlayer DMI strength is significant for harnessing its huge potential in spintronic devices. In 2024, Pai et al. demonstrated an efficient manipulation of interlayer DMI in magnetic multilayers by employing oblique angle deposition (OAD) technique to create wedge-shaped layers with opposing symmetry-breaking polarities[108]. Figure 9a provides a graphical representation of the counter-wedged structure. The corresponding R_H-H_z loop of the counter-wedged sample exhibits a clear hysteresis loop shift (Fig. 9b), which is dependent on the in-plane field's azimuthal direction φ_H. The magnitude of H_{offset} as a function of φ_H is summarized in Fig. 9c. Here, the angular dependence of H_{offset} can be described by the formula $H_{offset} = H_{DMI} \sin(\varphi_H\text{-}\varphi_D)$ (φ_D represents the azimuthal angle of the interlayer DMI vector $\boldsymbol{D}$). It can be seen the counter-wedge sample shows a maximum strength of H_{DMI} of 113.8 Oe. Therefore, the interlayer DMI strength can be optimized by engineering the multilayer structure.

In principle, both intralayer and interlayer DMI strengths are fixed after sample growth. However, from an application point of view, the post-growth manipulation of interlayer DMI is much more desirable to dynamically control the local 3D chiral spin-structure in spintronic devices. In 2023, Kläui et al. presented an intriguing interplay between electrical current and interlayer DMI in Ta(4)/Pt(4)/Co(0.6)/Pt(0.7)/Ru(0.8)/Pt(0.5)/Co(1)/Pt(4) (thicknesses in nanometers) SAF with PMA[109]. The optical image and measurement setup of Hall devices are given in Fig. 9d. Clearly, the chiral exchange biased hysteresis loops have been observed under positive and negative in-plane field of 100 mT (Fig. 9e). The angle dependence of switching field (H_{sw}) for FM_1 and FM_2 is also given in Fig. 9f, g, respectively. The unidirectional feature of interlayer DMI was observed. By analyzing the current dependence of the interlayer DMI effective field ($H_{IL\text{-}DMI}$) for FM_1 and FM_2 (Fig. 9g), both the strength of interlayer DMI changes and the phase of the sine function fit is shifted under higher current density. In addition to the growth-induced intrinsic interlayer DMI term, it was found that the current-induced effect leads to a second term with a cosine function.

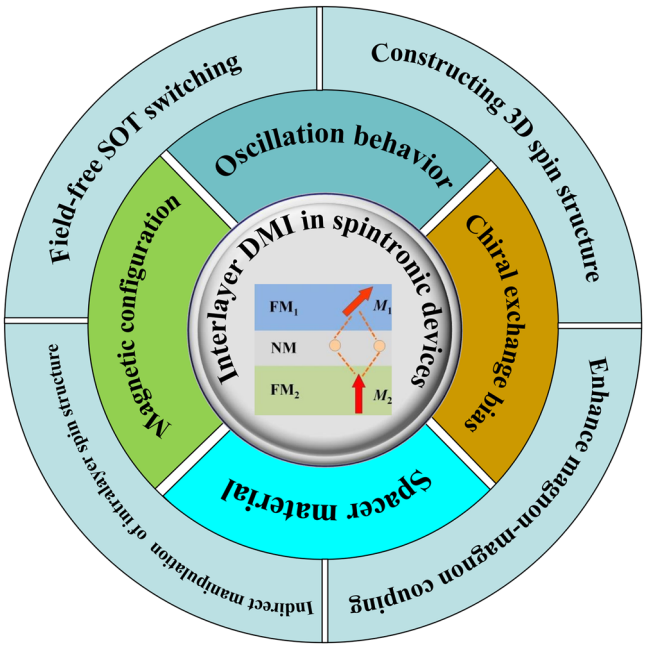

Fig. 10 | The basic characteristics and potential applications of interlayer DMI. Schematic illustration of the intriguing characteristics of interlayer DMI is listed, including oscillating behavior, chiral exchange bias and strong dependence on the spacer material and magnetic configuration. The broad applications in the spin-based logic and memory devices with novel functionality are also highlighted.

The detailed current density dependence measurements have revealed the fact that the current-induced contribution scales linearly with its current density and exhibits symmetry with current direction. Moreover, the magnitude of the current-induced contribution is comparable to the intrinsic term at experimentally manageable DC current densities, suggesting that an electrical current could directly manipulate the 3D chiral spin structure without the need of an external magnetic field.

Summary and outlook

Up until recently neglected in the framework of spintronics, both the theoretical and experimental works have revealed that DMI not only exists at magnetic interfaces but also across NM layers, owing to the spin-orbit scattering of conduction electrons in the HM layer or Rashba-type SOC. Figure 10 summarizes the intriguing progress in basic characteristics (inner circle), along with their application in spintronic devices (outer circle). The asymmetry of the hysteresis loops, i.e., chiral exchange bias, has been observed due to the inversion symmetry of magnetic reversal, which could be regarded characteristic effect of interlayer DMI. Meanwhile, the amplitude of interlayer DMI exhibits a strong dependence on the azimuthal angle, magnetization configuration, spacer layer, and even externally applied current. Both the unidirectional and biaxial anisotropies have been observed, depending on the specific material systems. The oscillation decay trend of the interlayer DMI strength as a function of spacer thickness has been confirmed, which has been proven to share the same oscillating period with RKKY. The strength of interlayer DMI tends to show the maximum magnitude in the case of canted or orthogonal alignment of magnetization. Although the obtained strength of interlayer DMI so far is still insufficient to significantly change the intralayer magnetic ordering due to competition with a strong direct exchange coupling and intralayer DMI, it is evidently effective in competition with RKKY coupling, thus co-defining the interlayer ordering.

From the point of view of application, the emergence of the antisymmetric counterpart of IEC, interlayer DMI, greatly expands the scope of DMI research. In contrast to the intralayer DMI that leads to chiral 2D spin structures confined within individual magnetic layers, the long-range interlayer DMI through the mediation of the NM spacer contributes to the emergence of 3D spin textures across the entire magnetic multilayer. The realization of systems integrating interlayer DMI also offers a pathway for the indirect control of asymmetric effects via the magnetic state of a neighboring layer, such as the motion of DWs and spin waves. Additionally, the antisymmetric interlayer DMI in the $FM_1/NM/FM_2$ trilayer structure introduces an additional symmetry breaking, which enables field-free deterministic SOT switching by following the symmetry law of $\boldsymbol{j}//\boldsymbol{D}$, providing a versatile platform for exploring all-electrically driven spintronic devices. Meanwhile, it has been predicted that interlayer DMI can break the rotational symmetry of SAF systems and enable to the emergence of ultrastrong magnon-magnon coupling. Moreover, the post-growth manipulation of the strength of interlayer DMI has been implemented by tuning the applied current density. Therefore, the exploitation of interlayer DMI paves the way for novel spin-based memory or logic devices with novel functionalities.

From a prospective view, some crucial issues still need to be addressed for advancing the practical application of interlayer DMI. Firstly, there is a natural competition between antisymmetric interlayer DMI and symmetric RKKY interaction. The strength of interlayer DMI obtained so far is still smaller than the RKKY interaction. Further exploration and optimization of interlayer DMI in various material systems are crucial to further strengthen the 3D spin structure. Additionally, a quantitative theoretical description of the current manipulation of the interlayer DMI effect remains elusive. Finally, further experimental efforts on the interlayer DMI facilitated ultrastrong magnon-magnon coupling are required to validate the theoretical predictions.

Data availability

Data sets generated during the current study are available from the corresponding author on reasonable request.

Received: 24 January 2025; Accepted: 28 May 2025;
Published online: 20 June 2025

References

1. Parkin, S. S. P. Systematic variation of the strength and oscillation period of indirect magnetic exchange coupling through the 3d, 4d, and 5d transition metals. *Phys. Rev. Lett.* **67**, 3598–3601 (1991).
2. Ruderman, M. A. & Kittel, C. Indirect exchange coupling of nuclear magnetic moments by conduction electrons. *Phys. Rev.* **96**, 99–102 (1954).
3. Yosida, K. Magnetic properties of Cu-Mn alloys. *Phys. Rev.* **106**, 893–898 (1957).
4. Kasuya, T. A theory of metallic ferro- and antiferromagnetism on Zener's model. *Prog. Theor. Phys.* **16**, 45–57 (1956).
5. Stiles, M. D. Interlayer exchange coupling. *J. Magn. Magn. Mater.* **200**, 322–337 (1999).
6. De Vries, J. J. et al. Exponential dependence of the interlayer exchange coupling on the spacer thickness in MBE-grown Fe/SiFe/Fe sandwiches. *Phys. Rev. Lett.* **78**, 3023–3026 (1997).
7. Zhuravlev, M. Y., Tsymbal, E. Y. & Vedyayev, A. V. Impurity-assisted interlayer exchange coupling across a tunnel barrier. *Phys. Rev. Lett.* **94**, 026806 (2005).
8. Yang, Q. et al. Ionic liquid gating control of RKKY interaction in FeCoB/Ru/FeCoB and $(Pt/Co)_2/Ru/(Co/Pt)_2$ multilayers. *Nat. Commun.* **9**, 991 (2018).
9. Wang, X. et al. E-field control of the RKKY interaction in FeCoB/Ru/FeCoB/PMN-PT (011) multiferroic heterostructures. *Adv. Mater.* **30**, 1803612 (2018).
10. Duine, R. A., Lee, K. J., Parkin, S. S. P. & Stiles, M. D. Synthetic antiferromagnetic spintronics. *Nat. Phys.* **14**, 217–219 (2018).
11. Chatterjee, J. et al. Novel multifunctional RKKY coupling layer for ultrathin perpendicular synthetic antiferromagnet. *Sci. Rep.* **8**, 11724 (2018).

12. Rimmler, B. H., Pal, B. & Parkin, S. S. P. Non-collinear antiferromagnetic spintronics. *Nat. Rev. Mater*. **10**, 109–127 (2025).
13. Dal Din, A., Amin, O. J., Wadley, P. & Edmonds, K. W. Antiferromagnetic spintronics and beyond. *npj Spintron.* **2**, 25 (2024).
14. Chen, R. et al. Reducing Dzyaloshinskii-Moriya interaction and field-free spin-orbit torque switching in SAFs. *Nat. Commun.* **12**, 3113 (2021).
15. Fernández-Pacheco, A. et al. Symmetry-breaking interlayer Dzyaloshinskii-Moriya interactions in SAFs. *Nat. Mater.* **18**, 679–684 (2019).
16. Han, D. S. et al. Long-range chiral exchange interaction in SAFs. *Nat. Mater.* **18**, 703–708 (2019).
17. Fert, A. Magnetic and transport properties of metallic multilayers. *Mater. Sci. Forum* **59**, 439–480 (1990).
18. Bogdanov, A. & Hubert, A. The properties of isolated magnetic vortices. *Phys. Stat. Sol. B* **186**, 527 (1994).
19. Tacchi, S. et al. Interfacial Dzyaloshinskii-Moriya interaction in Pt/CoFeB films: effect of the heavy-metal thickness. *Phys. Rev. Lett.* **118**, 147201 (2017).
20. Yang, H., Liang, J. & Cui, Q. First-principles calculations for Dzyaloshinskii-Moriya interaction. *Nat. Rev. Phys.* **5**, 43–61 (2023).
21. Dmitrienko, V. E. et al. Measuring the Dzyaloshinskii-Moriya interaction in a weak ferromagnet. *Nat. Phys.* **10**, 202–206 (2014).
22. Yang, H., Thiaville, A., Rohart, S., Fert, A. & Chshiev, M. Anatomy of Dzyaloshinskii-Moriya Interaction at Co/Pt interfaces. *Phys. Rev. Lett.* **115**, 267210 (2015).
23. Nesbet, R. K. Heisenberg exchange interaction of two Mn atoms. *Phys. Rev.* **135**, A460 (1964).
24. Bode, M. et al. Chiral magnetic order at surfaces driven by inversion asymmetry. *Nature* **447**, 190 (2007).
25. Vedmedenko, E. Y., Udvardi, L., Weinberger, P. & Wiesendanger, R. Chiral magnetic ordering in two-dimensional ferromagnets with competing Dzyaloshinsky-Moriya interactions. *Phys. Rev. B* **75**, 104431 (2007).
26. Benitez, M. J. et al. Magnetic microscopy and topological stability of homochiral Néel domain walls in a Pt/Co/AlO_x trilayer. *Nat. Commun.* **6**, 8957 (2015).
27. Yang, S. H., Naaman, R., Paltiel, Y. & Parkin, S. S. P. Chiral spintronics. *Nat. Rev. Phys.* **3**, 328–343 (2021).
28. Jiang, W. et al. Blowing magnetic skyrmion bubbles. *Science* **349**, 283–286 (2015).
29. Fert, A., Reyren, N. & Cros, V. Magnetic skyrmions: Advances in physics and potential applications. *Nat. Rev. Mater.* **2**, 17031 (2017).
30. Yu, G. et al. Room-temperature skyrmions in an antiferromagnet-based heterostructure. *Nano Lett.* **18**, 980–986 (2018).
31. Tokura, Y. & Kanazawa, N. Magnetic skyrmion materials. *Chem. Rev.* **121**, 2857–2897 (2021).
32. Roessler, U. K., Bogdanov, A. N. & Pfleiderer, C. Spontaneous skyrmion ground states in magnetic metals. *Nature* **442**, 797–801 (2006).
33. Yu, X. Z. et al. Real-space observation of a two-dimensional skyrmion crystal. *Nature* **465**, 901–904 (2010).
34. Fert, A., Cros, V. & Sampaio, J. Skyrmions on the track. *Nat. Nanotechnol.* **8**, 152–156 (2013).
35. Cui, Q., Zhu, Y., Liang, J., Cui, P. & Yang, H. Antiferromagnetic topological magnetism in synthetic van der Waals antiferromagnets. *Phys. Rev. B* **107**, 064422 (2023).
36. Vedmedenko, E. Y., Riego, P., Arregi, J. A. & Berger, A. Interlayer Dzyaloshinskii-Moriya interactions. *Phys. Rev. Lett.* **122**, 257202 (2019).
37. Lavrijsen, R. et al. Magnetic ratchet for three-dimensional spintronic memory and logic. *Nature* **493**, 647–650 (2013).
38. Fernández-Pacheco, A. et al. Three-dimensional nanomagnetism. *Nat. Commun.* **8**, 15756 (2017).
39. Lévy, P. M. & Fert, A. Anisotropy induced by nonmagnetic impurities in CuMn spin-glass alloys. *Phys. Rev. B* **23**, 4667–4690 (1981).
40. Matthies, T., Rózsa, L., Szunyogh, L., Wiesendanger, R. & Vedmedenko, E. Y. Interlayer and interfacial Dzyaloshinskii-Moriya interaction in magnetic trilayers: first-principles calculations. *Phys. Rev. Res.* **6**, 043158 (2024).
41. Tannous, C. & Gieraltowski, J. The Stoner-Wohlfarth model of ferromagnetism. *Eur. J. Phys.* **29**, 475 (2008).
42. Atherton, D. L. & Beattie, J. R. A mean field Stoner-Wohlfarth hysteresis model. *IEEE T. Magn.* **26**, 3059–3063 (1990).
43. Emori, S., Bauer, U., Ahn, S. M., Martinez, E. & Beach, G. S. Current-driven dynamics of chiral ferromagnetic domain walls. *Nat. Mater.* **12**, 611–616 (2013).
44. Ryu, K. S., Thomas, L., Yang, S. H. & Parkin, S. Chiral spin torque at magnetic domain walls. *Nat. Nanotechnol.* **8**, 527–533 (2013).
45. Je, S. G. et al. Asymmetric magnetic domain-wall motion by the Dzyaloshinskii-Moriya interaction. *Phys. Rev. B* **88**, 214401 (2013).
46. Lo Conte, R. et al. Role of B diffusion in the interfacial Dzyaloshinskii-Moriya interaction in Ta/$Co_{20}Fe_{60}B_{20}$/MgO nanowires. *Phys. Rev. B* **91**, 14433 (2015).
47. Yoshimura, Y. et al. Soliton-like magnetic domain wall motion induced by the interfacial Dzyaloshinskii-Moriya interaction. *Nat. Phys.* **12**, 157–161 (2016).
48. Garcia, J. P. et al. Magnetic domain wall dynamics in the precessional regime: influence of the Dzyaloshinskii-Moriya interaction. *Phys. Rev. B* **104**, 014405 (2021).
49. Shahbazi, K. et al. Domain-wall motion and interfacial Dzyaloshinskii-Moriya interactions in Pt/Co/Ir(t_{Ir})/Ta multilayers. *Phys. Rev. B* **99**, 094409 (2019).
50. Di, K. et al. Asymmetric spin-wave dispersion due to Dzyaloshinskii-Moriya interaction in an ultrathin Pt/CoFeB film. *Appl. Phys. Lett.* **106**, 052403 (2015).
51. Wang, K., Qian, L., Ying, S. C. & Xiao, G. Spin-orbit torque switching of chiral magnetization across a synthetic antiferromagnet. *Commun. Phys.* **4**, 10 (2021).
52. Guo, Y. et al. Effect of interlayer Dzyaloshinskii-Moriya interaction on spin structure in synthetic antiferromagnetic multilayers. *Phys. Rev. B* **105**, 184405 (2022).
53. Cascales Sandoval, M. A. et al. Observation and formation mechanism of 360° domain wall rings in synthetic anti-ferromagnets with interlayer chiral interactions. *Appl. Phys. Lett.* **123**, 172407 (2023).
54. Camosi, L. et al. Anisotropic Dzyaloshinskii-Moriya interaction in ultrathin epitaxial Au/Co/W(110). *Phys. Rev. B* **95**, 214422 (2017).
55. Shibata, K. et al. Large anisotropic deformation of skyrmions in strained crystal. *Nat. Nanotechnol.* **10**, 589–592 (2015).
56. Liang, S. et al. Ruderman-Kittel-Kasuya-Yosida-type interlayer Dzyaloshinskii-Moriya interaction in synthetic magnets. *Nano Lett.* **23**, 8690–8696 (2023).
57. Yun, J. et al. Anisotropic interlayer Dzyaloshinskii-Moriya interaction in synthetic ferromagnetic/antiferromagnetic sandwiches. *Adv. Funct. Mater.* **33**, 2301731 (2023).
58. Chen, R. et al. Anisotropic interlayer Dzyaloshinskii-Moriya interactions in synthetic ferromagnetic multilayers. *Sci. Bull.* **68**, 878–882 (2023).
59. Avci, C. O., Lambert, C. H., Sala, G. & Gambardella, P. Chiral coupling between magnetic layers with orthogonal magnetization. *Phys. Rev. Lett.* **127**, 167202 (2021).
60. Zhao, X. et al. Enhanced interlayer Dzyaloshinskii-Moriya interaction and field-free switching in magnetic trilayers with orthogonal magnetization. *APL Mater.* **12**, 041103 (2024).
61. Zhou, J. et al. Chiral interlayer exchange coupling for asymmetric domain wall propagation in field-free magnetization switching. *ACS nano* **17**, 9049–9058 (2023).
62. Gao, F. S. et al. Experimental evidence of the oscillatory behavior of the interlayer DMI effect. *Appl. Phys. Lett.* **123**, 192401 (2023).
63. Lin, C. Y. et al. Field-free spin-orbit torque switching via oscillatory interlayer Dzyaloshinskii-Moriya interaction for advanced memory applications. *ACS Mater. Lett.* **6**, 400–408 (2023).

64. Demiroglu, E., Hancioglu, K., Yavuz, I., Avci, C. O. & Deger, C. Oscillatory behavior of interlayer Dzyaloshinskii-Moriya interaction by spacer thickness variation. *Phys. Rev. B* **109**, 144422 (2024).
65. Arregi, J. A., Riego, P., Berger, A. & Vedmedenko, E. Y. Large interlayer Dzyaloshinskii-Moriya interactions across Ag-layers. *Nat. Commun.* **14**, 6927 (2023).
66. Torrejon, J. et al. Interface control of the magnetic chirality in CoFeB/MgO heterostructures with heavy-metal underlayers. *Nat. Commun.* **5**, 4655 (2014).
67. Pollard, S. D. et al. Bloch chirality induced by an interlayer Dzyaloshinskii-Moriya interaction in ferromagnetic multilayers. *Phys. Rev. Lett.* **125**, 227203 (2020).
68. He, W. et al. Field-free spin-orbit torque switching enabled by the interlayer Dzyaloshinskii-Moriya interaction. *Nano Lett.* **22**, 6857–6865 (2022).
69. Wang, Y., Xia, J., Wan, C., Han, X. & Yu, G. Ultrastrong magnon-magnon coupling in SAFs induced by interlayer Dzyaloshinskii-Moriya interaction. *Phys. Rev. B* **109**, 054416 (2024).
70. Li, Y. C., Huang, Y. H., Huang, C. C., Liu, Y. T. & Pai, C. F. Field-free switching in symmetry-breaking multilayers: the critical role of interlayer chiral exchange. *Phys. Rev. Appl.* **20**, 024032 (2023).
71. Wang, Z. et al. Field-free spin-orbit torque switching of synthetic antiferromagnet through interlayer Dzyaloshinskii-Moriya interactions. *Cell Rep. Phys. Sci.* **4**, 101334 (2023).
72. Liu, L. Q. et al. Spin-torque switching with the giant spin Hall effect of tantalum. *Science* **336**, 555–558 (2012).
73. Miron, I. M. et al. Perpendicular switching of a single ferromagnetic layer induced by in-plane current injection. *Nature* **476**, 189–193 (2011).
74. Han, J., Cheng, R., Liu, L., Ohno, H. & Fukami, S. Coherent antiferromagnetic spintronics. *Nat. Mater.* **22**, 684–695 (2023).
75. Zhang, H. C. et al. Integration of high-performance spin-orbit torque MRAM devices by 200-mm-wafer manufacturing platform. *J. Semicond.* **43**, 102501 (2022).
76. Cubukcu, M. et al. Ultra-fast perpendicular spin-orbit torque MRAM. *IEEE Trans. Magn.* **54**, 9300204 (2018).
77. Khang, N. H. D., Ueda, Y. & Hai, P. N. A conductive topological insulator with large spin Hall effect for ultralow power spin-orbit torque switching. *Nat. Mater.* **17**, 808–813 (2018).
78. Haazen, P. P. J. et al. Domain wall depinning governed by the spin Hall effect. *Nat. Mater.* **12**, 299–303 (2013).
79. Zhu, L., Ralph, D. C. & Buhrman, R. A. Spin-orbit torques in heavy-metal-ferromagnet bilayers with varying strengths of interfacial spin-orbit coupling. *Phys. Rev. Lett.* **122**, 077201 (2019).
80. Miron, I. M. et al. Current-driven spin torque induced by the Rashba effect in a ferromagnetic metal layer. *Nat. Mater.* **9**, 230–234 (2010).
81. Peng, S. Z. et al. Exchange bias switching in an antiferromagnet/ferromagnet bilayer driven by spin-orbit torque. *Nat. Electron.* **3**, 757–764 (2020).
82. Yu, G. Q. et al. Switching of perpendicular magnetization by spin-orbit torques in the absence of external magnetic fields. *Nat. Nanotechnol.* **9**, 548–554 (2014).
83. Kang, M. G. et al. Electric-field control of field-free spin-orbit torque switching via laterally modulated Rashba effect in Pt/Co/AlO_x structures. *Nat. Commun.* **12**, 7111 (2021).
84. Jeong, J., Park, Y. S., Kang, M. G. & Park, B. G. Nanosecond magneto-ionic control of magnetism using a resistive switching HfO_2 gate oxide. *Adv. Electron. Mater.* **11**, 2400535 (2024).
85. Akyol, M. et al. Current-induced spin-orbit torque switching of perpendicularly magnetized Hf|CoFeB|MgO and Hf|CoFeB|TaO_x structures. *Appl. Phys. Lett.* **106**, 162409 (2015).
86. Fukami, S., Zhang, C., DuttaGupta, S., Kurenkov, A. & Ohno, H. Magnetization switching by spin-orbit torque in an antiferromagnet-ferromagnet bilayer system. *Nat. Mater.* **15**, 535–541 (2016).
87. Brink, A. et al. Field-free magnetization reversal by spin-Hall effect and exchange bias. *Nat. Commun.* **7**, 10854 (2016).
88. Lau, Y. C., Betto, D., Rode, K., Coey, J. M. D. & Stamenov, P. Spin-orbit torque switching without an external field using interlayer exchange coupling. *Nat. Nanotechnol.* **11**, 758–762 (2016).
89. Wang, X. et al. Field-free programmable spin logics via chirality-reversible spin-orbit torque switching. *Adv. Mater.* **30**, 1801318 (2018).
90. Kurenkov, A., Zhang, C., DuttaGupta, S., Fukami, S. & Ohno, H. Device-size dependence of field-free spin-orbit torque induced magnetization switching in antiferromagnet/ferromagnet structures. *Appl. Phys. Lett.* **110**, 092410 (2017).
91. Wang, M. X. et al. Field-free spin-orbit torque switching via out-of-plane spin-polarization induced by an antiferromagnetic insulator/heavy metal interface. *Nat. Commun.* **14**, 2871 (2023).
92. Wu, H. et al. Chiral symmetry breaking for deterministic switching of perpendicular magnetization by spin-orbit torque. *Nano lett.* **21**, 515–521 (2020).
93. Fan, H. D. et al. Field-free spin-orbit torque switching in synthetic ferro and antiferromagents with exchange field gradient. *Adv. Funct. Mater.* **33**, 2211953 (2023).
94. Liu, L., Song, Y., Zhao, X., Liu, W. & Zhang, Z. Full-scale field-free spin-orbit torque switching in HoCo structure with a vertical composition gradient. *Adv. Funct. Mater.* **32**, 2200328 (2022).
95. Zheng, Z. Y. et al. Field-free spin-orbit torque-induced switching of perpendicular magnetization in a ferromagnetic layer with a vertical composition gradient. *Nat. Commun.* **12**, 4555 (2021).
96. Huang, X. H. et al. Implementing versatile programmable logic functions using two magnetization switching types in a single device. *Adv. Funct. Mater.* **34**, 2308219 (2023).
97. Chen, J. L. et al. Strong interlayer magnon-magnon coupling in magnetic metal-insulator hybrid nanostructures. *Phys. Rev. Lett.* **120**, 217202 (2018).
98. MacNeill, D. et al. Gigahertz frequency antiferromagnetic resonance and strong magnon-magnon coupling in the layered crystal $CrCl_3$. *Phys. Rev. Lett.* **123**, 047204 (2019).
99. Li, Y. et al. Coherent spin pumping in a strongly coupled magnon-magnon hybrid system. *Phys. Rev. Lett.* **124**, 117202 (2020).
100. Shiota, Y., Taniguchi, T., Ishibashi, M., Moriyama, T. & Ono, T. Tunable magnon-magnon coupling mediated by dynamic dipolar interaction in synthetic antiferromagnets. *Phys. Rev. Lett.* **125**, 017203 (2020).
101. Sud, A. et al. Tunable magnon-magnon coupling in synthetic antiferromagnets. *Phys. Rev. B* **102**, 100403 (2020).
102. Li, M., Lu, J. & He, W. Symmetry breaking induced magnonmagnon coupling in synthetic antiferromagnets. *Phys. Rev. B* **103**, 064429 (2021).
103. Liensberger, L. et al. Exchange-enhanced ultrastrong magnon-magnon coupling in a compensated ferrimagnet. *Phys. Rev. Lett.* **123**, 117204 (2019).
104. Makihara, T. et al. Ultrastrong magnon-magnon coupling dominated by antiresonant interactions. *Nat. Commun.* **12**, 3115 (2021).
105. Sud, A., Yamamoto, K., Suzuki, K. Z., Mizukami, S. & Kurebayashi, H. Magnon-magnon coupling in synthetic ferrimagnets. *Phys. Rev. B* **108**, 104407 (2023).
106. Vedmedenko, E. Y. & Kostylev, M. Boundary conditions for and ferromagnetic resonance spectra of magnetic bilayers coupled by interlayer Dzyaloshinskii-Moriya interactions. *Phys. Rev. Appl.* **23**, 014047 (2025).
107. Yang, Z., Liu, C., Yang, X. & Zhang, Y. Influence of local Dzyaloshinskii-Moriya interaction on spin waves in symmetrical heavy metal/ferromagnet/heavy metal multilayer. **58**, 03LT03 (2024).
108. Huang, Y. H. et al. Tailoring interlayer chiral exchange by azimuthal symmetry engineering. *Nano Lett.* **24**, 649–656 (2024).
109. Kammerbauer, F. et al. Controlling the interlayer Dzyaloshinskii-Moriya interaction by electrical currents. *Nano Lett.* **23**, 7070–7075 (2023).

Acknowledgements
The work was supported by the Research Start-up Funds of Hangzhou International Innovation Institute of Beihang University under Grant 2024KQ01, Guangdong Provincial Key Laboratory Project (High-Performance Integrated Circuits and Systems Laboratory, No. 2023KSYS003).

Author contributions
X.P. Zhao wrote the main text of the manuscript and provided funding. J.H. Zhao provided supervision, discussion and funding. All authors contributed to the writing of the manuscript.

Competing interests
The authors declare no competing interests.

Additional information
Correspondence and requests for materials should be addressed to Jianhua Zhao.